Proceedings of the 21st ICSMGE, Vienna, Austria, 14 – 19 June 2026. Pistrol, Adam & Schweiger (eds.)
Published by: ÖGG, Austrian Society for Geomechanics, Salzburg, Austria, ISBN 978-3-9503898-4-5
https://doi.org/10.53243/ICSMGE2026-995

Poisson's effects on the compression and tension shaft capacity of piles in weak rocks

Yuchen Yang, Tingfa Liu, Andrea Diambra, George Mylonakis
School of Civil, Aerospace and Design Engineering, University of Bristol, Bristol, UK; yuchen.yang@bristol.ac.uk

ABSTRACT: Piles driven in fine-grained soils are generally thought to develop identical tensile and compressive shaft capacities. However, piles driven in non-cohesive or free-draining soils may develop notably higher shaft capacities under compression than tension, as recognised from full-scale field pile tests in sands and, more recently, in low-to-medium density chalk. Modern 'CPT-based' axial capacity methods for driven piles in sands typically incorporate tension-to-compression shaft capacity ratios of less than unity (≈ 0.7-0.8), while a lower ratio of 0.5 has recently been recommended by the ALPACA-SNW method for low-to-medium density chalks. Poisson's effects have been recognised as a key factor contributing to differences in compression and tension shaft capacities, as pile shafts develop radial Poisson strains that increase or decrease radial effective stresses particularly when interacting with stiff surrounding geomaterials. This paper reports on the development of analytical solutions to investigate how Poisson's effects may depend on pile geometry (i.e. slenderness and wall thickness ratios), ground stiffness profiles, and stiffness contrast between the pile materials and the surrounding rock masses. Illustrative examples are presented of two field pile tests in chalk. The outcomes have important implications for designing pile foundations or caissons for jacket structures, tension-leg platforms or other station-keeping systems where significant tension loading may be expected in their full life cycles.

KEYWORDS: Poisson's effects, pile foundations, shaft capacity, surrounding geomaterials.

1 INTRODUCTION

Tubular piles or caissons of various slenderness and wall thickness are employed extensively in jacket foundations for supporting bottom-fixed offshore structures or as parts of station-keeping system for floating platforms or wind turbines (FOWTs). Tension capacity may dominate the design for these loading scenarios where limited reliance can be made on piles' base resistances. It is often accepted that piles installed in fine-grained undrained clays develop broadly identical shaft capacities under tensile loading (pull-out) and compressive loading (push-in). However, in non-cohesive or free-draining soils, early field tests reviewed by De Nicola & Randolph (1993) suggested that shaft capacities under tension could be moderately lower than those under compression, primarily due to effects of principal stress axis rotation and 'Poisson' straining of the pile steel. Modern CPT-based design approaches, for example the ICP-05 (Jardine et al., 2005) and the 'unified' (Lehane et al., 2020) methods, account for differences between tension and compression shaft capacities by incorporating an average loading factor (or coefficient) of ≈ 0.75. Lower ratios have been reported in literature that may reflect variations in pile geometries and ground conditions.

Significant differences in tension and compression shaft capacities were recently identified for chalk, a variable, porous, weak biomicrite limestone widespread (Mortimore, 2012). Jardine et al. (2024) reviewed available field tests of large tubular steel piles driven at UK, French and German chalk sites and concluded that shaft capacities in compression could be much higher than those in tension by a factor of two, as shown in Figure 1. A constant tension-to-compression ratio of 0.5 is incorporated explicitly in their ALPACA-SNW method with loading factors of 2/3 and 4/3 respectively for piles under tension and compression.

This paper extends the earlier studies by De Nicola & Randolph (1993) and Alawneh et al. (2007) on driven piles in sands and presents theoretical formulations and solutions for assessing Poisson's ratio effects on tension and compression shaft capacities of piles driven in weak rocks. Parametric studies and illustrative examples of two ALPACA test piles are presented that investigate the effects of pile geometries (slenderness and wall thickness ratios), ground stiffness profiles, and stiffness contrast between pile materials and surrounding rock masses. The theoretical derivations and solutions are also applicable for piles installed in noncohesive soils and other weak or hard rocks by impact driven, drilled-and-grouted and other methods.

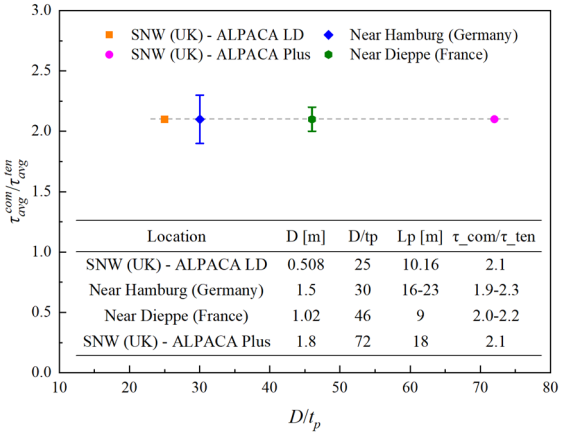

Location	D [m]	D/tp	Lp [m]	τ_com/τ_ten
SNW (UK) - ALPACA LD	0.508	25	10.16	2.1
Near Hamburg (Germany)	1.5	30	16-23	1.9-2.3
Near Dieppe (France)	1.02	46	9	2.0-2.2
SNW (UK) - ALPACA Plus	1.8	72	18	2.1

Figure 1. Compression-to-tension shaft capacity ratios determined from field pile tests at chalk sites (adopted from Jardine et al., 2024)

2 THEORETICAL DERIVATION

The derivation considers a vertical hollow open-ended cylindrical steel pile with embedded length L, outer radius r_p and wall thickness t_p. The pile is assumed to behave elastically with a Young's modulus E_p and Poisson's ratio ν_p. The surrounding soil or rock mass is assumed to be a uniform elastic-perfectly plastic frictional material characterised by an operational elastic shear modulus G_{ope}, a pile-to-soil interface friction angle δ and cone resistance q_t, which collectively set an upper bound for pile shaft shear resistances. Any plug or internal soil column is considered separately. The pile shaft is subjected to a pre-existing radial effective stress σ_{rc}' from combined geostatic and installation-induced stresses. An additional dilation-induced stress component $\Delta\sigma_{rd}'$ is considered. The σ_{rc}' and $\Delta\sigma_{rd}'$ components are calculated based on the ALPACA-SNW method proposed by Jardine et al. (2024), as are end bearing resistance q_b and pile base capacity Q_b under compression. Any residual stress or reversed end bearing is not modelled explicitly. Seepage and excess pore water pressure are likewise ignored.

2.1 *Steel pipe pile under compression loading*

Considering a segment of a laterally unconfined cylindrical pipe pile under an axial compression load P_z in Figure 2, the axial, circumferential and radial strains (ε_a, ε_θ and ε_r, respectively) developed can be determined as:

$$\varepsilon_a = \frac{\sigma_a}{E_p} = \frac{P_z}{E_p A_p} \tag{1}$$

$$\varepsilon_r = \varepsilon_\theta = -\nu_p\, \varepsilon_a = -\nu_p \left(\frac{P_z}{E_p A_p}\right) \tag{2}$$

$$\varepsilon_r = \varepsilon_\theta = \frac{\Delta D}{D_0} = \frac{u}{r_p} \tag{3}$$

where σ_a is axial stress; A_p and E_p are pile's cross-sectional area and Young's modulus, respectively; ν_p is pile Poisson's ratio; ΔD is change in pile diameter after expansion; D_0 is initial pile diameter; r_p is pile outer radius. The pile periphery's free lateral expansion, u, can be established by combing Equations (2) and (3) as:

$$u = -\nu_p r_p \left(\frac{P_z}{E_p A_p}\right) \tag{4}$$

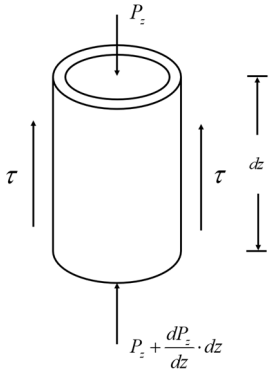

Figure 2. Pile segment and the associated stresses under compression.

As shown in Figure 3 (upper plot), considering part of the free radial expansion is inhibited by the surrounding soil with certain stiffness, the pile's radial displacements can be determined by introducing the expressions of soil lateral stiffness (Vesic, 1972) and pile lateral stiffness (Cook and Young, 1999) through the following expressions:

$$K_s = \frac{2G_s}{r_p} \tag{5}$$

$$K_p = \frac{E_p t_p}{r_p^2} \tag{6}$$

$$K_p u_2 = K_s u_1 \tag{7}$$

$$u_1 = u - u_2 \tag{8}$$

where K_s is the lateral stiffness of the surrounding soil in uniform expansion (measured in units of Force per Length^3); G_s is soil shear modulus; K_p is the corresponding stiffness of the pile cross section; t_p is pile wall thickness; u_1 is the actual pile lateral expansion; $u_2 = u - u_1$ is the difference between the hypothetical (reference) expansion of the unconfined pile (u) and the (smaller) actual pile expansion (u_1), due to the restraining action of surrounding soil.

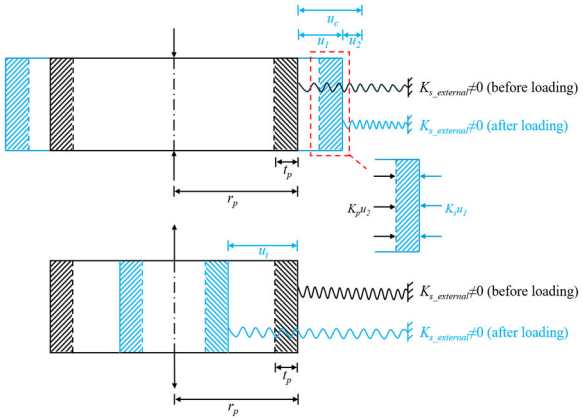

Figure 3. Poisson's straining induced radial displacements under compressive (upper plot) and tensile (lower plot) axial pile load.

Substituting Equations (5), (6) and (7) into Equation (8) leads to the following solution for u_2:

$$u_2 = -\nu_p r_p \left(\frac{P_z}{E_p A_p}\right)\left[1 + \frac{E_p}{2G_s}\frac{t_p}{r_p}\right]^{-1} \tag{9}$$

Evidently, the constrained pile radial displacement (expansion) leads to increases in horizontal effective stress ($\Delta\sigma_{hl}$) normal to pile shaft and consequently shear stress ($\Delta\tau_{hl}$) along the shaft:

$$\Delta\sigma_{hl} = K_s u_1 = K_p u_2 \tag{10}$$

$$\Delta\tau_{hl} = \Delta\sigma_{hl} \tan\delta_f = -\nu_p \tan\delta_f \left(\frac{P_z}{A_p}\right)\left[\frac{E_p}{2G_s} + \frac{r_p}{t_p}\right]^{-1} \tag{11}$$

where δ_f is friction angle at the pile-soil interface at ultimate conditions. Note that the shear stress increment ($\Delta\tau_{hl}$) varies with along pile shaft. Rearranging Equation (11) and considering the force equilibrium of the pile segment in the vertical direction, the shear stress at failure τ_f can be determined as:

$$-\frac{t_p}{\nu_p \tan\delta_f}\left[\frac{d(\Delta\tau_{hl})}{dz}\left(\frac{E_p}{2G_s} + \frac{r_p}{t_p}\right) + \Delta\tau_{hl}\frac{E_p}{2}\frac{d}{dz}\left(\frac{1}{G_s}\right)\right] = \tau_f \tag{12}$$

2.2 *Steel pipe pile under tension loading*

Under tension loading, the pile develops a contraction displacement (u) and the reduction in pile diameter is not restricted by the surrounding soil (see the lower plot in Figure 3). The corresponding circumferential strain and displacement can be expressed as:

$$\varepsilon_\theta = \frac{2\pi(r_p - u) - 2\pi r_p}{2\pi r_p} = -\frac{u}{r_p} \tag{13}$$

$$u = \nu_p r_p \left(\frac{P_z}{E_p A_p}\right) \tag{14}$$

The consequent decrease in radial effective stress is:

$$\Delta\sigma_{hl} = K_s u \tag{15}$$

Decrease in shear stress due to Poisson's straining can be defined as:

$$\Delta\tau_{hl} = \nu_p \tan\delta_f G_s \left(\frac{2P_z}{E_p A_p}\right) \tag{16}$$

Further rearrangement and differentiation lead to shear stress at failure τ_f as:

$$\frac{E_p t_p}{2\nu_p \tan\delta_f}\left[\frac{d(\Delta\tau_{hl})}{dz}\frac{1}{G_s}+\Delta\tau_{hl}\frac{d}{dz}\left(\frac{1}{G_s}\right)\right]=\tau_f \quad (17)$$

The above solution assumes free radial contraction and neglects any additional resistance to contraction due to the presence of internal soil column or plug, in similar ways as Alawneh et al. (2007) considered for piles in sands. Yang et al. (2025) present a set of improved analytical solutions that incorporate 'internal' soil stiffness along pile shaft length to match practical scenarios more faithfully.

2.3 *Solutions*

A fourth-order Runge-Kutta method (Cortell, 1993) was adopted in this study with the initial-value problem being defined as:

$$f(z,y)=\frac{d(\Delta\tau_{hl})}{dz}, \Delta\tau_{hl}(z_0)=\Delta\tau_{hl}^0, z_0=L \quad (18)$$

Rearranging Equations (12) and (17) leads to the following expressions for implicit differential equations of changes in shear stress along the pile shaft due to Poisson's effect, under compressive and tensile load respectively:

$$\frac{d(\Delta\tau_{hl})_c}{dz}=-\frac{\tau_f\frac{\nu_p\tan\delta_f}{t_p}+\Delta\tau_{hl}\frac{E_p}{2}\frac{d}{dz}\left(\frac{1}{G_s}\right)}{\frac{E_p}{2G_s}+\frac{r_p}{t_p}} \quad (19)$$

$$\frac{d(\Delta\tau_{hl})_t}{dz}=\frac{\tau_f\frac{2\nu_p\tan\delta_f}{E_p t_p}+\Delta\tau_{hl}\frac{d}{dz}\left(\frac{1}{G_s}\right)}{\frac{1}{G_s}} \quad (20)$$

2.4 *Determination of pile shaft capacity*

The CPT-based ALPACA-SNW method (Jardine et al., 2024) for axial shaft capacity of driven piles in low-to-medium density chalk was applied to calculate the shear stresses at failure in Equations (19) and (20). Other empirical or theoretical correlations may be applied for different geomaterials concerned.

$$\tau_f=f_L(\sigma'_{rc}+\Delta\sigma'_{rd})\tan\delta_f \quad (21)$$

$$\Delta\sigma'_{rd}=\frac{4G_{ope}\Delta r}{D} \quad (22)$$

Above water table,

$$\frac{\sigma'_{rc}}{q_t}=f_{tip}\times 0.078\times\left(\frac{h}{r_p}\right)^{-0.85}\quad\left(\frac{h}{r_p}\geq 4.0\right) \quad (23)$$

Below water table,

$$\frac{\sigma'_{rc}}{q_t}=f_{tip}\times 0.025\times\left(\frac{h}{r_p}\right)^{-0.80}\quad\left(\frac{h}{r_p}\geq 0.5\right) \quad (24)$$

Where f_L is a loading factor taken as 2/3 and 4/3 for tension and compression respectively. $\Delta\sigma'_{rd}$ is change in radial effective stress due to interface dilation; σ'_{rc} is stationary radial effective stress after installation and prior to loading; G_{ope} is operational shear modulus taken as 1/4 of the maximum in-situ shear stiffness G_{max}; D is pile diameter; Δr is radial dilation at pile interface taken as ≈ 5μm and ≈ 3μm above and below water table, respectively; f_{tip} is pile tip condition factor, taken as 1 for open-ended condition and 3 for close-ended condition; q_t is CPT resistance; h is the distance to pile tip.

The compression-to-tension shaft capacity ratio, Q_c/Q_t, can be written as:

$$\frac{Q_c}{Q_t}=\frac{Q_0+\Delta Q_c}{Q_0-\Delta Q_t} \quad (25)$$

$$Q_0=2\pi r_p\int_0^L(\sigma'_{rc}+\Delta\sigma'_{rd})\tan\delta_f dz \quad (26)$$

where Q_0 is shaft capacity for an infinitely rigid pile (without Poisson's straining) determined from Equation (26) by taken f_L as unity; ΔQ_c and ΔQ_t are respectively changes in compression and tension shaft capacity due to Poisson's effects, as calculated by integrating the shear stresses in Equations (19) and (20).

3 EXAMPLE CASES AND DISCUSSIONS

The above formulae and solutions were developed in a Python programme to facilitate parametric study. The ALPACA LD and ALPACA Plus TP1 pile tests reported by Jardine et al. (2024) (see Figure 1) are considered here. Profiles of operational shear stiffness and cone resistance adopted in the analysis are shown in Figure 4. Table 1 summarises the pile geometries and the coefficients of power law functions fitting the operational chalk shear stiffness profiles.

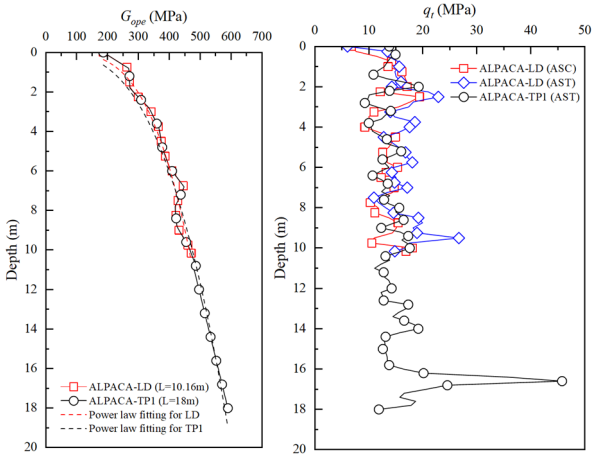

Figure 4. G_{ope} and q_t profiles adopted in the analysis (AST: Axial Static Tension; ASC: Axial Static Compression).

Table 1. Pile geometries and chalk stiffness profiles

Pile	L [m]	D [m]	L/D	t_p [mm]	D/t_p	G_{ope} [MPa] ($G_{ope}=a\times z^b$)
LD	10.2	0.508	20	20.6	25	a=261.8, b=0.24
TP1	18.0	1.8	10	25.0	72	a=245.6, b=0.29

Notes: E_p adopted as 200 GPa, δ_f as 32° and ν_p as 0.3.

The effects of the stiffness of the surrounding soil mass on compression-to-tension shaft capacity ratios are shown in Figure 5, in which G_{ave} represents average soil shear modulus along the pile shaft length (from z = 0 to L) and varies up to 1 GPa in the analysis. The Young's modulus of steel pile E_p is set as a constant of 200 GPa. Pile geometries and chalk properties are listed in Table 1. As indicated in Equations (12), (17), (19) and (20), soil shear modulus G dominates the magnitude of the Poisson's straining. The compression-to-tension ratios of the larger diameter, lower slenderness ratio TP1 pile appear to be more sensitive to the variations in soil stiffness. Figure 6 demonstrates how the compression-to-tension ratios vary as pile wall thickness changes while maintaining pile outer diameter, length and chalk properties. It is observed that Q_c/Q_t ratios increase with pile wall thickness ratio (D/t_p) and the LD and TP1 trends converge to close to unity as the D/t_p ratio decreases to 2, which represents solid closed-ended conditions. Table 2 summarises the measured and predicted tension and

compression shaft capacities and the resultant Q_c/Q_t ratios, indicating broadly compatible outcomes and validating the proposed analytical models and solutions. It is noted that the current solution does not consider the stiffness of internal soil column (or plug), which impacts particularly the larger diameter pile TP1. Further refinement is presented in Yang et al. (2025).

Table 2. Summary of measured and calculated shaft capacities and Q_c/Q_t capacity ratios for ALPACA LD and TP piles (field data from Jardine et al. (2024)).

Pile	Method	Q_c [kN]	Q_t [kN]	Q_c/Q_t
LD	Field	1142	595-634	1.9
LD	ALPACA-SNW	1329	654-780	1.7-2.0
LD	Analytical	1687	918	1.8
TP1	Field	12109	5766	2.1
TP1	ALPACA-SNW	11930	5964	2.0
TP1	Analytical	14222	5055	2.6

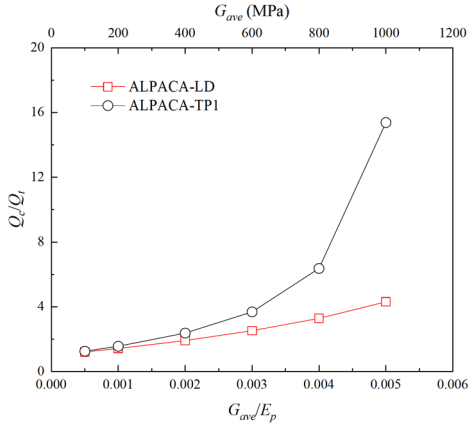

Figure 5. Effect of soil-pile stiffness ratio on shaft capacity ratio.

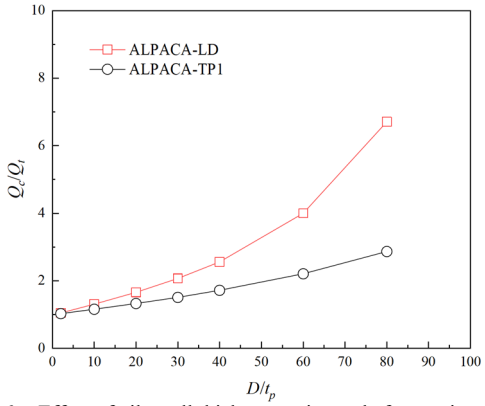

Figure 6. Effect of pile wall thickness ratio on shaft capacity ratio.

4 CONCLUSIONS

Tubular piles or caissons are routinely designed to sustain tension loading in a wide range of offshore applications. This study draws on recent pile testing campaigns and development of CPT-based design methods and develops analytical solutions for assessing Poisson's effects on tension and compression shaft capacities of piles driven in weak rocks. Key conclusions drawn from the study are:

(1) When subjected to axial tension or compression loading, steel piles develop radial Poisson's straining that leads to increase or decrease in radial effective stress and therefore pile shaft capacity.
(2) The proposed analytical model and solutions can capture the key factors affecting Poisson's effects, including pile slenderness and wall thickness ratios, ground stiffness profiles, and stiffness contrast between the pile materials and surrounding media.
(3) The example pile cases show broadly consistent outcomes between the analytical solutions and field measurements. Combined effects of pile geometry and soil stiffness conditions are identified that can lead to substantially lower shaft capacity in tension than in compression.

The current analytical model and solutions employed operational stiffness to represent the mass stiffness of the surrounding media without considering installation induced heterogeneities and any radial variations of rock properties as observed by Vinck et al. (2025) and others. Further development is required to model installation effects explicitly.

5 ACKNOWLEDGEMENTS

This first Author gratefully acknowledges the financial support by the China Scholarship Council (CSC) - University of Bristol (UoB) joint Doctoral Scholarship.

6 REFERENCES

Alawneh, A.S., Nusier, O.K., and Sharo, A.A. 2007. Poisson's ratio effect on compressive and tensile shaft capacity of driven piles in sand: Theoretical formulation. *Computers and Geotechnics*, 34(3), 151-163.

Cerfontaine, B., White, D., Kwa, K., Gourvenec, S., Knappett, J., and Brown, M. 2023. Anchor geotechnics for floating offshore wind: Current technologies and future innovations. *Ocean Engineering*, 279, 114327.

Cortell, R. 1993. Application of the fourth-order Runge-Kutta method for the solution of high-order general initial value problems. *Computers & structures*, 49(5), 897-900.

Cook, R. D., and Young, W. C. 1999. *Advanced mechanics of materials*.

Coyle, H.M., and Castello, R.R. 1981. New design correlations for piles in sand. *Journal of the Geotechnical Engineering Division*, 107(7), 965-986.

De Nicola, A., and Randolph, M.F. 1993. Tensile and compressive shaft capacity of piles in sand. *Journal of geotechnical engineering*, 119(12), 1952-1973.

Jardine, R., Chow, F., Overy, R., and Standing, J. 2005. *ICP Design methods for driven piles in sands and clays*. London: Thomas Telford Ltd

Jardine, R., Buckley, R.M., Liu, T., Andolfsson, T., Byrne, B.W., Kontoe, S., Mcadam, R.A., Schranz, F., and Vinck, K. 2024. The axial behaviour of piles driven in chalk. *Géotechnique*, 74(6), 553-569.

Lehane, B.M., Liu, Z., Bittar, E., Nadim, F., Lacasse, S., Jardine, R., Carotenuto, P., Rattley, M., Gavin, K., and More Authors. 2020. A new 'unified' CPT-based axial pile capacity design method for driven piles in sand. *Proc. 4th International Symposium on Frontiers in Offshore Geotechnics*, Austin, 462-477.

Liu, T., Vinck, K., Jardine, R., Kontoe, S., and Buckley, R.M. 2025. The reliability of axial design methods for open steel piles driven in chalk. *Journal of Geotechnical and Geoenvironmental Engineering*, 151(12).

Liu, T., Vinck, K., Ushev, E.R., and Jardine, R. 2024. In-situ and laboratory characterisation of stiff and dense geomaterials for driven pile analysis and design. *Soils and Rocks*, 47(3).

Mortimore, R.N. 2012. Making sense of Chalk: a total-rock approach to its Engineering Geology. *Quarterly Journal of Engineering Geology and Hydrogeology*, 45(3), 252-334.

Vesić, A.S. 1972. Expansion of cavities in infinite soil mass. *Journal of the soil Mechanics and Foundations Division*, 98(3), 265-290.

Vinck, K., Liu, T., Jardine, R., and Buckley, R.M. 2025. Characterising the damage developed around piles by percussive driving in low-to-medium density chalk. *Proc. 5th International Symposium on Frontiers in Offshore Geotechnics*, Nantes.

Yang, Y., Liu, T., Mylonakis, G., and Diambra, A. 2025. Poisson's effects on the shaft capacity of driven piles in weak rocks. Under review.